Cell Tissue Res (2017) 369:413–427
DOI 10.1007/s00441-017-2592-1

REGULAR ARTICLE

Dynamic of contribution of UBPy-sorted cargo to acrosome biogenesis: effects of its derailment in a mouse model of globozoospermia, the infertile Vps54 (L967Q) mutant

Mariarosa Gioria[1] · **Maria Enrica Pasini**[1] · **Giovanna Berruti**[1]

Received: 9 November 2016 / Accepted: 21 February 2017 / Published online: 15 March 2017

Abstract The sperm acrosome is a specialized vacuole, a member of the family of cell-specific lysosome-related organelles. Its exocytosis, the acrosome reaction, is a crucial event during fertilization. The released acrosomal contents promote sperm penetration through the investments of the oocyte, whereas the membranous components of the acrosome are involved in sperm-oocyte interaction/fusion and oocyte activation. The way that these functionally distinct acrosomal costituents reach the vacuole during its biogenesis remains poorly understood. The biosynthetic pathway and a consistent supply from the endosomal system have recently been documented. We use immunogold electron microscopy to determine the contribution of endosome cargo-sorting during step-by-step mouse acrosomogenesis. The chosen proteins of this study were UBPy (ESCRT-DUB), together with endosome compartment markers EEA1 and pallidin. The latter is described here for the first time in male germ cells. This new insight expands our knowledge of acrosomogenesis, confirming the plasticity of the endosomal system in supporting cell-type-specific functions. We also study wobbler mice, whose Vps54 mutation causes motor neuron degeneration and male infertility. Use of electron/immunoelectron microscopy and immunofluorescence enabled us to establish that the lack of an acrosome in wobbler spermatozoa is attributable to an early block in acrosome biogenesis and that the mislocalization of acrosome-destined proteins, potentially involved in the signaling events leading to oocyte activation, is possibly responsible for wobbler infertility, even after intracytoplasmic sperm injection.

Keywords Acrosome · Lysosome-related organelle · Endosome compartment · De-ubiquitinating enzyme · Globozoospermia

Introduction

The mammalian spermatozoon is a highly specialized cell that, in order to fulfill its fundamental role, i.e., the fertilization of an oocyte, needs two peculiar sperm-specific organelles, namely the flagellum and the acrosome. The latter is a large vacuole located at the tip of the sperm head and its shape typifies the cell morphology in hook-shaped (rodents) and spatulatae (human, bovine, porcine) spermatozoa. Both the structure and function of the acrosome deserve attention because of the compartmentation of the components of the acrosome, consistent with the succession of the progressive and distinct roles it plays at fertilization (Berruti 2016). Described for decades as a direct Golgi derivative, the present concept of the acrosome as a novel lysosome-related organelle (LRO) is acquiring growing experimental support (Berruti and Paiardi 2011, 2015; Guyonnet et al. 2012; Wang et al. 2014). LROs comprise a group of cell-type-specific membranous organelles that share features with endosomes and lysosomes but that exhibit, albeit partially, a unique composition, morphology and structure (Marks et al. 2013). LROs progressively mature from precursors that can differ in origin by acquiring specialized cargoes so as to generate membranous and lumenal environments conducive for the function that the specific LRO has to accomplish (Raposo and Marks 2007; Meng et al. 2012). The acrosome also develops through sequential phases (Golgi, cap, acrosomal, maturation) from a precursor (Moreno

✉ Giovanna Berruti
giovanna.berruti@unimi.it

[1] Department of Biosciences, Unversity of Milan, Via Celoria 26, 20133 Milan, Italy

et al. 2000); the precursor, according to the hypothesis of the acrosome as a LRO (Berruti and Paiardi 2011), lies in the so-called "acrosomal granule", which forms during the Golgi phase by the coalescence of scattered, not well defined, proacrosomal granules. The spermatid endocytic system contributes to acrosomal development at least during entry into the cap phase (Berruti et al. 2010; Berruti and Paiardi 2015); at the acrosome and maturation phase, respectively, the luminal content gradually condenses (Hardy et al. 1991) and the acrosomal shape changes becoming thinner, in particular at the equatorial segment, so as to acquire its streamlined features (Buffone et al. 2008). The complexity of acrosomogenesis, which lasts about 2 weeks in the mouse and 1 month in the human, makes it susceptible to various defects that may be detrimental for male fertility.

To achieve successful fertilization, the acrosome not only undergoes the acrosome reaction, a mandatory step (Yanagimachi 2011) but also provides sperm-borne factors essential for sperm-oocyte fusion (Satouh et al. 2012) and/or involved in oocyte activation (Ito et al. 2010). Acrosomeless spermatozoa, such as those of wobbler mice (Paiardi et al. 2011), fail to fertilize oocytes, even after ICSI (intracytoplasmic sperm injection; Heytens et al. 2010), probably because the lack of an acrosome makes the spermatozoa deficient for oocyte activation (Vanden Meerschaut et al. 2013).

To investigate acrosome biogenesis at a deep ultrastructural level, we sought to localize, by employing immunoelectron microscopy, intracellular proteins known to work at the endocytic/LRO route-pathway. One of the proteins that we investigated is UBPy (Gnesutta et al. 2001), a de-ubiquitylase otherwise known as Usp8, which we have previously shown to control acrosome biogenesis (Berruti and Martegani 2005; Berruti et al. 2010; Berruti and Paiardi 2015). Mutations in the *Usp8* gene might account for some cases of unexplained infertility in the human population (Kosova et al. 2012). The other proteins investigated here are canonical components of the endocytic/LRO system, such as EEA1 and pallidin (Berruti et al. 2010; Dell'Angelica 2004). The study was additionally extended to wobbler acrosomogenesis. Taking our data together, we provide here new knowledge about a topic for which information is still rather scanty.

Materials and methods

Animals

Testes and epididymes were isolated from CD1 male mice purchased from Charles River Italia (Calco, Lecco, Italy). Wobbler mice and healthy littermates (NFR strain, NIH, Animal Resources, Bethesda, USA) were provided by Drs. Tiziana Mennini and Paolo Bigini ("Mario Negri" Institute for Pharmacological Research, Milano, Italy) and were bred at Charles River Italia (Paiardi et al. 2014). Mice were housed at a temperature of 21 ± 1 °C with a relative humidity of 55 ± 10 % and a 12 h light/dark cycle. Genotypization of the progeny from mating heterozygous male and female mice was carried out as described (Paiardi et al. 2014). Only homozygous wobbler (wr/wr) and control mice (+/+) were used. Animals used as organ donors were killed by carbon dioxide asphyxiation at selected times. All animal protocols used herein were carried out with authorization from the Ethical Committee for Animal Experimentation of the University of Milan and by the Italian Ministry of Health and in compliance with the animal care requirements as set by Italian law (Law D.L. 27.1.1992 n. 116, in agreement with European Union directive 86/609/CEE) and with the NIH Guide for the Care and Use of Laboratory Animals. All efforts were made to minimize the number of animals used.

Antibodies

Primary antibodies were as follows: rabbit anti-mUBPy/USP8 (as described by Gnesutta et al. 2001), mouse monoclonal anti-EEA1 (BD Transduction Laboratories, Mississauga, ON, Canada), rabbit anti-pallidin (Proteintech Group, Chicago, Ill., USA) and mouse monoclonal anti-MET (Santa Cruz Biotechnology, Santa Cruz, Calif., USA). Secondary antibodies used for immunogold electron microscopy (goat anti-rabbit IgG or anti-mouse IgG conjugated with 5- and 15-nm gold particles) were from British Biocell International (Cardiff, UK). Secondary antibodies used for immunofluorescence (goat anti-rabbit IgG Alexa Fluor488 or Alexa Fluor568 and goat anti-mouse IgG Alexa Fluor488) were from Invitrogen (Leek, The Netherlands).

Isolation of spermatogenic cells and spermatozoa for immunoblotting and indirect immunofluorescence analysis

Spermatogenic cells were isolated from testes and spermatozoa were collected from epididymes as described (Berruti et al. 2010; Paiardi et al. 2011). Cell lysates subjected to pallidin immunoblotting were then obtained and processed as reported previously (Berruti and Paiardi 2015). For immunofluorescence analysis, 4 % (v/v) paraformaldehyde-fixed ice-cold acetone-postfixed preblocked spermatogenic cells/spermatozoa were immunostained with the indicated primary antibodies followed by the appropriate Alexa-488-conjugated, Alexa 568-conjugated or, in the case of double-immunolabeling, a mixture of the appropriate secondary antibodies. Counterstaining of nuclei was carried out with Draq5 (5 μM; Biostatus, Shepshed, UK) or 4,6-diamidino-2-phenylindole (DAPI; 2 μg/ml; Sigma-Aldrich Chemical). Cells were examined in a Leica TCS SPAOBS scanning laser confocal fluorescent microscope (Leica Laserteknik,

Heidelberg, Germany) equipped with an Ar/Kr (488 nm) laser, He/Ne (568 nm) laser, and UV (361–365 nm) laser for green, red and blue fluorescence, respectively. Captured images (Leica Power Scan software) were elaborated with Adobe Photoshop (Mountain View, Calif., USA).

Transmission electron microscopy

Whole testes were removed and immediately immersed in 3 % glutaraldehyde in 0.1 M phosphate buffer (PB), pH 7.2–7.4. After 30 min, the samples were cut into small pieces (2–3 mm^3) and placed in the same fresh fixative for 4 h at room temperature. Samples were washed in buffer, postfixed in 2 % osmium tetroxide in 0.1 M PB (pH 7.2–7.4) for 2 h at 4 °C, dehydrated in a graded ethanol series followed by propylene oxide and embedded in Epoxy resin. In order to assess the preservation and orientation of seminiferous tubules, some semithin sections (1 μm) were stained with toluidine blue and examined by light microscopy. Ultrathin sections (70 nm) of the area of interest were cut by using a diamond knife on a Reichert Ultracut ultramicrotome, mounted on Cu/Rh grids (200 mesh), contrasted with uranyl acetate and lead citrate, observed and photographed via a Zeiss 902 transmission electron microscope operating a 80 kV. Negative films were acquired at a resolution of 600 dpi by means of an Epson PERFECTION V700 PHOTO scanner.

Immunogold electron microscopy

Whole testes were fixed in a mixture of 1.5 % glutaraldehyde and 3.5 % paraformaldehyde (electron microscope grade) in 0.1 M PB, pH 7.4. After 30 min, the samples were cut into small pieces (2–3 mm^3) and placed in the same fixative for 4 h at 4 °C. After being washed in 0.1 M PB, the samples were treated with 0.05 M NH_4Cl for 30 min to quench free aldehyde groups, washed in buffer, dehydrated in a graded ethanol series and embedded in acrylic LR White resin (London Resin, England; Ted Pella, Redding, Calif., USA). Following polymerization at 50 °C for 24 h, ultrathin sections (70 nm) were cut with a diamond knife on a Reichert Ultracut ultramicrotome and collected on 200 mesh nickel grids. The sections were incubated in blocking solution by floatation of the grids on drops of 0.05 M TRIS-buffered saline (TBS) pH 7.2 containing 1 % bovine serum albumin (BSA) for 30 min at room temperature and incubation overnight at 4 °C in a humidified chamber in specific primary antibody diluted in 0.05 M TBS pH 7.2 containing 0.1 % BSA. The following primary antibodies were used: anti-mUBPy/USP8 (1:300), anti-EEA1 (1:25), anti-pallidin (1:100). Primary antibodies were removed by extensive washing on drops of TBS (4 × 10 min/each). The grids were then transferred for 1 h to drops of the appropriate secondary antibody conjugated with 5- or 15-nm gold particles by using a 1:50 working dilution in TBS containing 1 % BSA. For double-immunolabeling, grids were incubated overnight in a mixture of the selected primary antibodies. Bound antibodies were revealed by a mixture of the appropriate secondary antibodies conjugated with gold particles of different diameters (5- and 15-nm, respectively). After extensive washes in TBS, sections were finally rinsed in double-distilled water and then counterstained with aqueous uranyl acetate and lead citrate. As a negative control, some grids were processed in the same way but with omission of the primary antisera. Specimens were observed and photographed via a Zeiss 902 transmission electron microscope operating at 80 kV. Negative films were acquired at a resolution of 600 dpi by means of an Epson PERFECTION V700 PHOTO scanner.

Results

Dynamic distribution of UBPy in spermatids undergoing acrosomogenesis

Internalization of plasma membrane proteins, in particular receptor tyrosine kinases (RTKs), is promoted by a series of events involving, in the early endosome, the first endocytic hub (Marks et al. 2013). The early endosome compartment, however, contains a variety of vesicular intermediates including tubular endosomes; in LRO-containing cells, the latter sort the cargo from the early endosome toward the newly forming LRO (Meng et al. 2012). The endosome de-ubiquitylase UBPy has profound effects on endosome morphology and organization (Mizuno et al. 2006) and in the down-regulation of membrane receptors (Berruti and Martegani 2005; Ceriani et al. 2015).

We recently showed that, during acrosomogenesis, UBPy is involved in the recruitment of the RTK MET toward the forming acrosome (Berruti and Paiardi 2015). Here, we localized UBPy and, indirectly, UBPy-sorted cargo, for the first time at the ultrastructural level, by UBPy-immunogold electron microscopy. Figure 1 summarizes the localization of UBPy-positive cargo in round spermatids that are at the early cap phase. UBPy-positive vesicle-like (Fig. 1, arrows) and tubular-like (Fig. 1, arrowheads) structures were detected at the subplasmalemmal region and inside the spermatid cytoplasm and UBPy-positive material resembling that observed in the cytoplasm was detected in close contact with the acrosomal membrane and/or inside the acrosome (Fig. 1a–c). Conversely, the Golgi apparatus with its horseshoe shape and cis-compartment facing the cell periphery was negative for immunogold UBPy labeling (Fig. 1d, e).

The acrosome in cap-phase spermatids at later stages of development is characterized by fold-like extensions of the membrane now partitioned into an outer (distal, toward the cell periphery) and inner (proximal, toward the nucleus) membrane. In general, in such spermatids, UBPy-immunogold

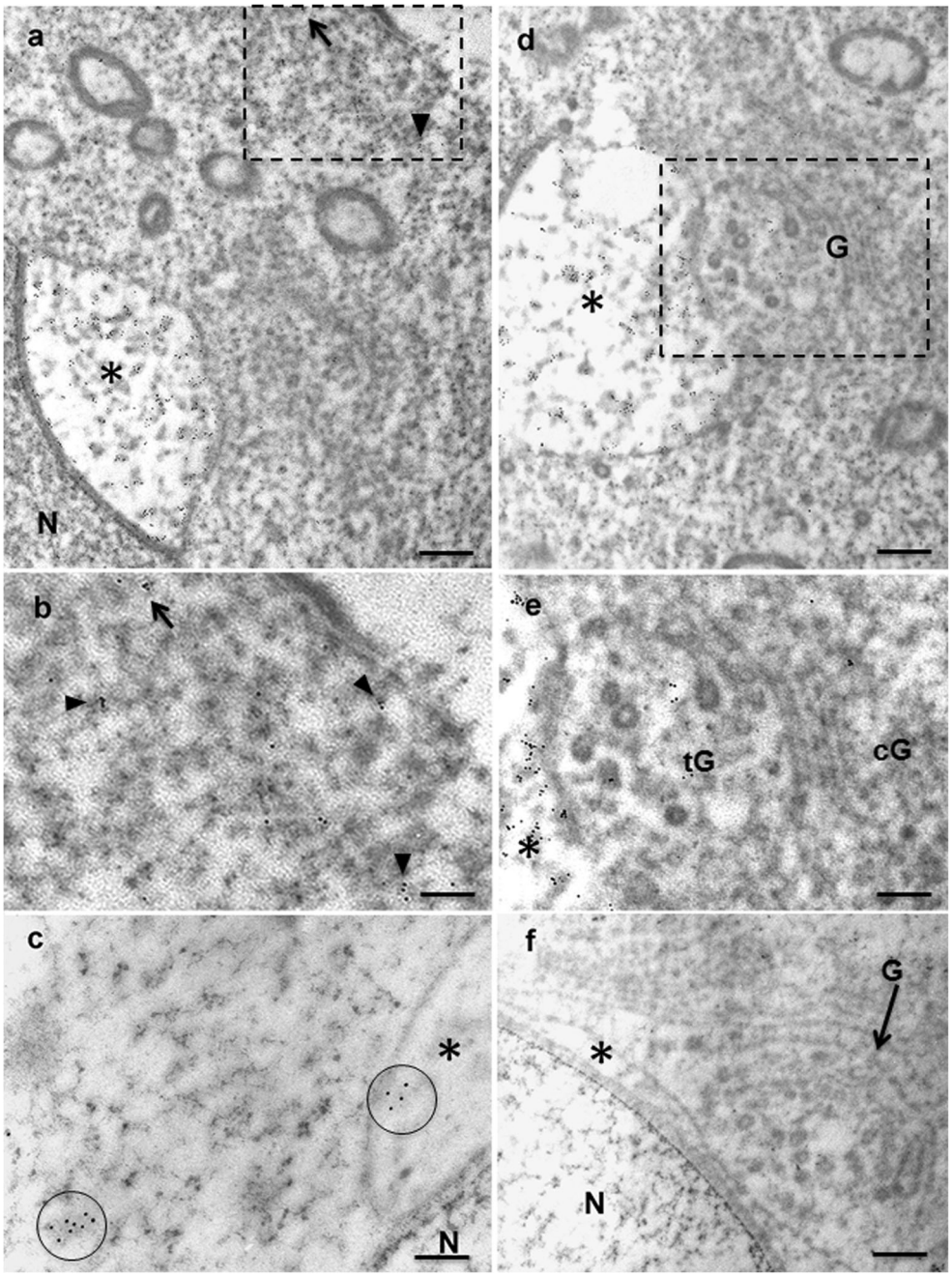

Fig. 1 Localization of UBPy in early cap-phase spermatids by immunogold-electron microscopy. **a**, **b** UBPy-positive vesicle-like (*arrows*) and tubular-like (*arrowheads*) structures are present at the sub-plasmalemmal region, in the cytoplasm and inside the developing acrosome (*asterisk*). **b** Higher magnification of *boxed area* in **a**. *Bars* 0.5 μm (**a**), 0.2 μm (**b**). **c** Immunogold particles (*circles*) mark tubular structures detected both in the cytoplasm and at the acrosome (*N* nucleus, *asterisk* acrosome). *Bar* 0.3 μm. **d**, **e** Portion of a step 4 spermatid showing that the Golgi apparatus (*G*) is devoid of immunogold particles, both at the cis (*cG*) and middle/trans (*tG*) compartment, whereas UBPy labeling is present in the proximity of and inside the acrosome (*asterisk*). **e** Higher magnification of *boxed area* in **d**. *Bars* 0.5 μm (**d**), 0.2 μm (**e**). **f** Similar portion of a cap phase spermatid immunostained only with the secondary gold-conjugated antibody as a control (*N* nucleus, *G* Golgi apparatus, *asterisk* acrosome). *Bar* 0.5 μm

labeling was found to associate with the acrosomal membranes, in particular the fold-like extensions (Fig. 2). UBPy-positive material was, however, still found when about to fuse with the outer acrosomal membrane (Fig. 2b) and inside the cytoplasm. Again, Golgi saccules and/or cisternae showed no immunoreactivity (Fig. 2b). To ascertain further the endosomal origin of the UBPy-positive material, we checked for EEA1 (early endosome antigen 1) positivity by immunogold electron microscopy. EEA1-immunostained structures, starting from coated pits to tubular vesicles/electron-dense material resembling the UBPy-positive structures, were revealed at the plasma membrane, inside the cytoplasm and near to/within the acrosome of cap-phase spermatids (Fig. 3a–c). The experimental approach of using gold particles of different sizes enabled us to provide contemporary double UBPy/EEA1 immunogold staining. As can be appreciated in Fig. 3d–f, UBPy and EEA1 were found to colocalize on the same early endosomes, albeit at non-overlapping domains. Therefore, an evaluation of our findings suggests a consistent and dynamic contribution of the endosomal UBPy-sorted cargo to the forming acrosome in cap-phase spermatids.

The flattening and elongation of the acrosome and of the nucleus below are hallmarks of the acrosomal and maturation

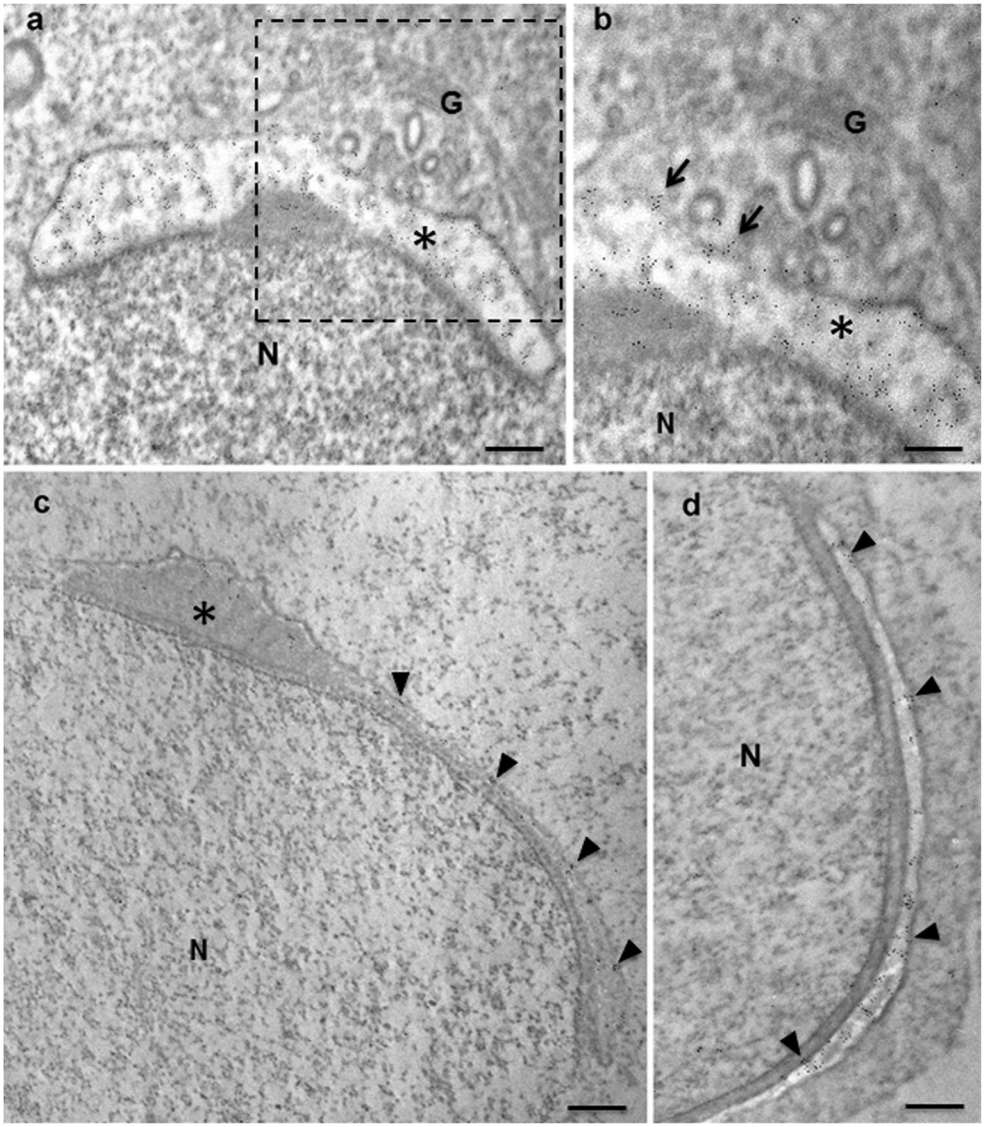

Fig. 2 Localization of UBPy in late cap-phase spermatids by immunogold-electron microscopy. **a**, **b** Numerous clusters of gold particles are present at the level of the acrosome (*asterisk*), which flattens over the nucleus (*N*). The cisternae of the Golgi apparatus (*G*) are always negative for UBPy (*arrows* clusters of immunogold particles on the cytoplasmic side of the outer acrosomal membrane). **b** Higher magnification of *boxed area* in **a**. *Bars* 0.5 μm (**a**), 0.2 μm (**b**). **c**, **d**. Spermatids in the late cap-phase (step 7). UBPy immunoreactivity is detectable on both of the acrosomal membranes along the fold-like extensions (*arrows*) spreading over the nucleus (*N*). *Bars* 0.5 μm

phases of acrosomogenesis. The UBPy immunolabeling documented such an evolving pattern of cellular shape/protein distribution. At the acrosomal phase, immunoreaction accumulated at the acrosome outlining the profiles of the outer and inner acrosomal membranes, whereas the condensing acrosomal matrix was devoid of immunogold particles (Fig. 4a–c). UBPy immunoreaction was also persistently observed in the region consistent with the presence of the manchette, in close opposition to the post-acrosomal nuclear envelope (Fig. 4b, c). The manchette is a transient microtubule structure that forms just beneath the acrosome and wraps up the spermatid nucleus so as to promote its elongation and then disappears (Kierszenbaum and Tres 2004). The UBPy association with the manchette is not surprising because UBPy contains an MIT (microtubule interacting and trafficking) domain at its amine-terminus; this has previoulsy been shown to be able to interact with spermatid microtubule arrays (Berruti et al. 2010; Berruti and Paiardi 2015). The UBPy acrosomal immunolabeling pattern that has evolved during the acrosomal phase of spermatid development is maintained in spermatids at the maturation phase (Fig. 4d–f).

Involvement of pallidin in acrosome biogenesis

BLOC-1 (biogenesis of lysosome-related organelles complex-1) is critical for LRO biogenesis by sorting cargoes from early endosomes to the forming LRO (Falcón-Pérez et al. 2002; Lee et al. 2012; Meng et al. 2012). BLOC-1 contains eight protein subunits including pallidin, gene mutations of which are responsible for HPS7–9 (Hermansky-Pudlak syndrome; Li et al. 2004; Cullinane et al. 2011) and neurological disorders (Spiegel et al. 2015). Pallidin is known to localize to early endosomes by its interaction with the early endosome t-SNARE syntaxin-13 (Cullinane et al. 2011).

As further validation of the nature of the sperm acrosome as a LRO, we searched for pallidin/BLOC-1 in spermatids.

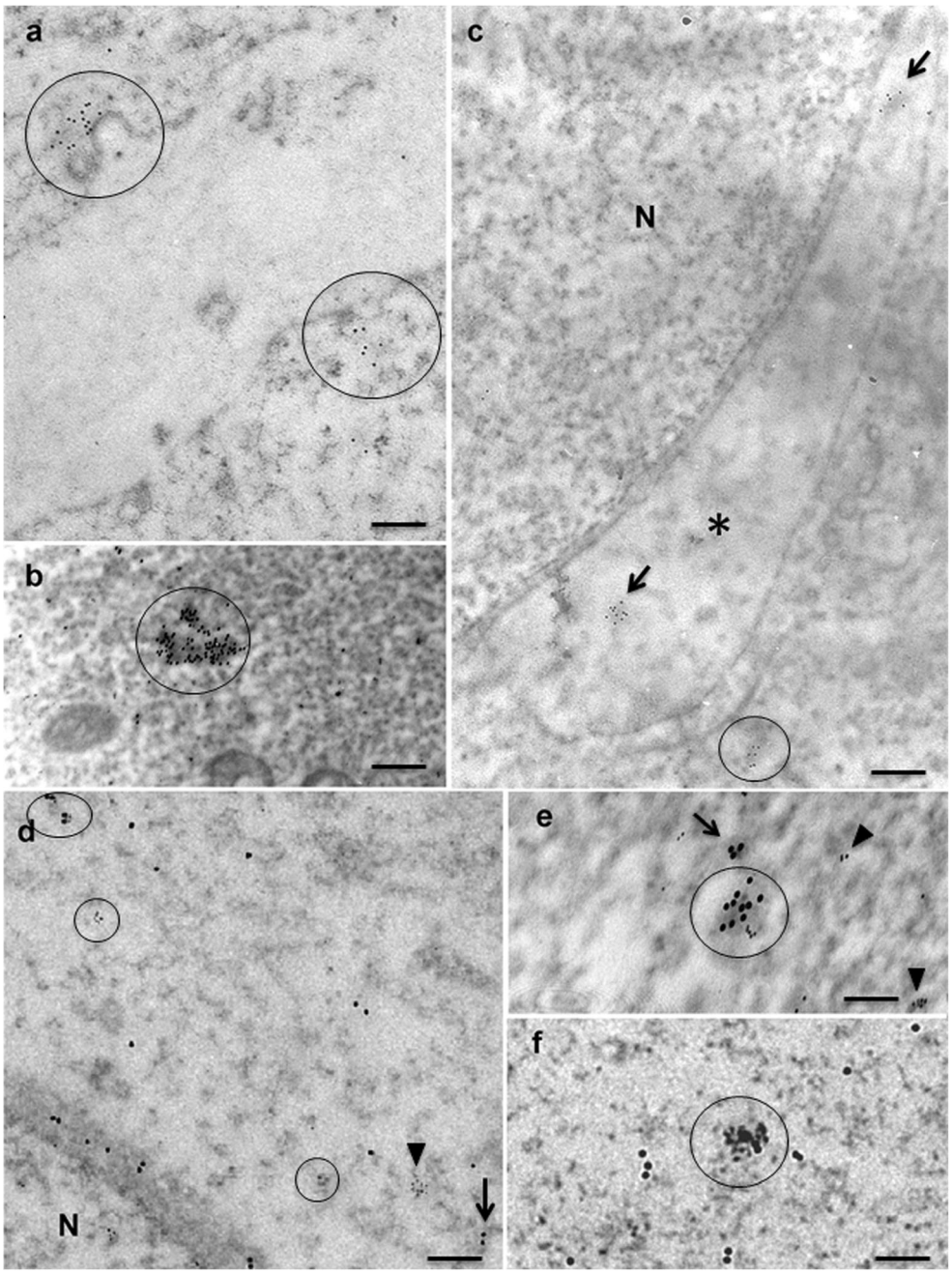

Fig. 3 EEA1 and EEA1/UBPy double-immunostaining in acrosome-developing spermatids. **a** Immunolabeling for EEA1 shows coated pits (*circles*) at the sub-plasmalemmal region of two facing round spermatids. *Bar* = 0.2 μm. **b**, **c** Tubular profiles intensely labeled for EEA1 are detected in the cytoplasm, near the forming acrosome (*circles*) and inside (*arrow*) the acrosome (*asterisk)*. *Bars* = 0.2 μm. **d–f** Double UBPy (15-nm gold)/EEA1 (5-nm gold) immunolabeled spermatids. In the cytoplasm, gold in the two sizes is present not only on distinct structures (*arrows*, *arrowheads*, respectively) but also on the same vesicle/tubular-like structures (*circles*). *Bars* 0.3 μm (**d**), 0.15 μm (**e**, **f**)

Notably, the presence of pallidin has never been investigated in male germ cells. Therefore, to test for the presence of pallidin, protein extracts from male germ cell suspensions were assayed by Western immunoblot. As shown (Fig. 5b), a band of approximately 25 kDa, the predicted molecular weight for pallidin (Meng et al. 2012), was specifically recognized by the anti-pallidin antibody in the soluble protein fraction recovered from both a milder (lane 1) and strong (lane 2) detergent treatment. Such antibodies were then used for immunofluorescence analysis of fresh spermatid cell suspensions. Scattered pallidin-positive fluorescent puncta were observed in round spermatids (Fig. 5a) with an immunostaining pattern reminiscent, at least in part, of that previously reported for UBPy and EEA1 (Berruti et al. 2010). Based on these findings, we performed further immune-electron microscopy. Pallidin immunogold staining yielded highly reproducible results in sections obtained from various testis samples. Representative images are provided in Fig. 5. In early and late cap phase spermatids, labeling was detected predominantly in cytoplasmic tubulovesicular structures with morphologic characteristics of early endosomes/sorting endosomes and inside the forming acrosome (Fig. 5c, d). The Golgi apparatus was devoid of labeling. Pallidin was still detected in acrosomal (Fig. 5e) and maturation (Fig. 5f, g) phase spermatids with

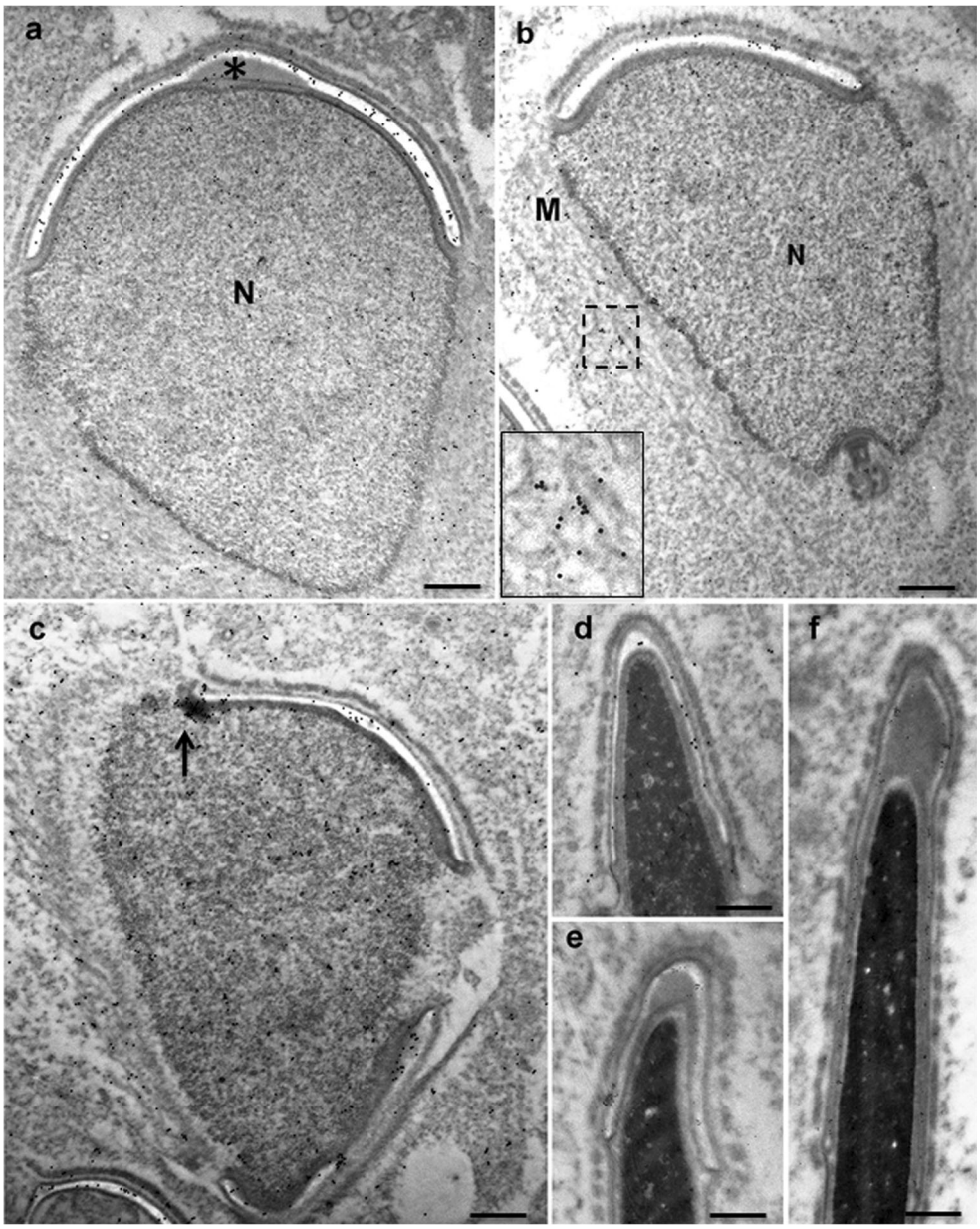

Fig. 4 Immunogold localization of UBPy in riper developing spermatids. **a** Spermatid in acrosomal phase (step 8): immunogold particles associate mostly with the acrosomal membranes of the flattening and elongating acrosome. *Bar* 1 μm. **b** In step 9 spermatids, immunogold particles outline the profiles of the outer and inner acrosomal membranes. Discrete UBPy immunostaining is visible on the manchette (*M*), a transient microtubular structure that begins to form in step 8 spermatids. The manchette consists in ordered microtubule bundles with a role in sculpting sperm head shape and in mediating trafficking process for the assembly of the sperm tail. *Inset* Higher magnification of a portion of the UBPy-immunolabeled manchette. *Bar* 1 μm (**b**), 0.3 μm (*inset*). **c** Elongating spermatid (step 11) sectioned at an oblique angle. UBPy labeling follows the contour of the developing acrosome (*arrow* intensely marked posterior marginal ring). *Bar* 1 μm. **d–f** Spermatids at maturation-phase (various sections). Anti-UBPy immunogold labels the outer and inner acrosomal membranes, whereas the condensed acrosomal matrix is devoid of labeling. *Bar* 0.5 μm

immunogold particles being concentrated predominantly at the acrosomal membrane profiles. Together, these data indicate the intrinsic nature of LRO for the sperm acrosome.

Wobbler acrosomogenesis

The Wobbler mouse, best known as a model of motor neuron degeneration (Boillée et al. 2002), also represents a valid model for globozoospermia with its sperm being characterized by the lack of a true acrosome, which is anomalously condensed and a deformed nucleus, plus an irregularly formed and shaped tail (Heimann et al. 1991; Paiardi et al. 2011; Jockusch et al. 2014). Although Wobbler spermiogenesis has previoulsy been documented by electron microscopic observations (Heimann et al. 1991), the ultrastructural analysis was carried out before the gene mutation responsible for the wobbler phenotype had been identified, i.e., a point mutation in the *Vps54* gene (Schmitt-John et al. 2005). *Vps54* encodes a vesicular protein-sorting retrograde factor involved in the tethering from endosomes to the *trans* Golgi network (Quenneville et al. 2006).

We performed an electron microscopy study taking into consideration, in particular, the spermatid vesicular compartment of the wobbler mouse. First, wobbler testes from 34-day-old mice were examined. As the first spermatogenic wave with spermiation ends at day 35 of age, we reasoned that this stage would enable us to detect spermatids differentiating up until the spermatozoa next to be released. The images provided in Fig. 6 are representative of shared patterns from three

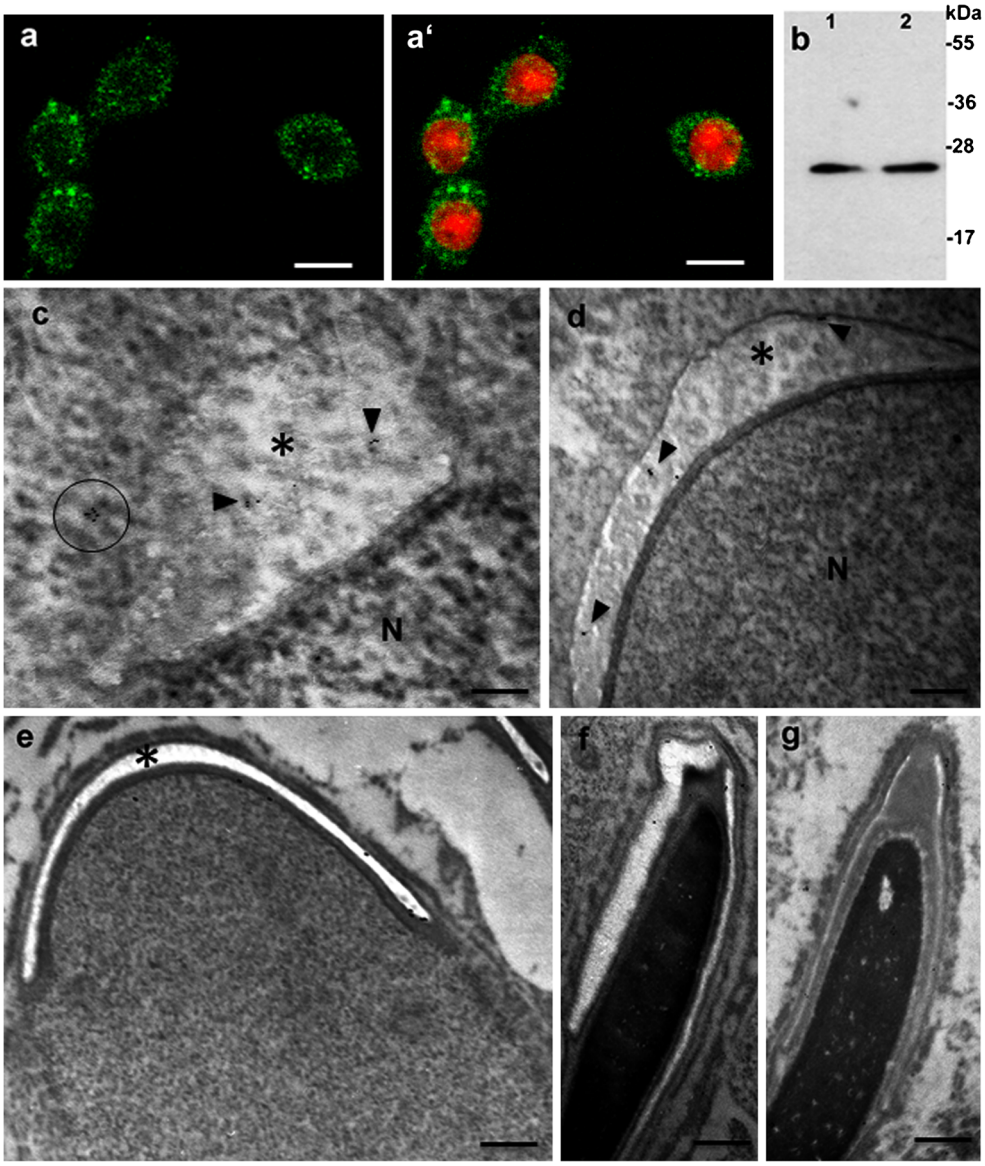

Fig. 5 Evidence for the presence of pallidin in mouse spermatids. **a**, **a'** Round spermatids fluorescently labeled for pallidin (**a**, *green*) and pallidin merged with a signal for DNA (**a'**, *red*). *Bar* 1.5 μm. **b** Triton X-100 (*lane 1*) and RIPA buffer (*lane 2*) protein lysates from spermatogenic cells immunoblotted for anti-pallidin. *Right* Molecular markers. **c-g** Ultrastructural immunogold localization of pallidin in developing spermatids. Spermatid at early cap-phase (**c**) exhibits pallidin on vesicular structures (*circle*) close to the acrosome (*asterisk*) and in inside the acrosome (*arrowheads).* *Bar* 0.2 μm. Spermatid in late cap-phase (**d**) with pallidin immunolabeling (*arrowheads)* inside the acrosome (*asterisk*). *Bar* 0.2 μm. Spermatids in acrosomal (**e**) and maturation (**f**, **g**) phases: immunogold particles are distributed along the acrosomal membrane profiles. *Bars* 0.5 μm

different wobbler mice. Low-magnification micrographs (Fig. 6a, b) provide a general picture of the apical compartment of the seminiferous epithelium to reveal the principal defects of wobbler spermiogenesis, i.e., the lack of a true acrosome, of head flattening/elongation and the presence of an abnormal tail. In addition, we report developmental anomalies previously not described. A constant finding was the presence, in stage VII/VIII spermatids, of a greater number of acrosomal granules contacting the nuclear envelope (Fig. 6d, e). Such granules sometimes delineated the entire nuclear circumference (Fig. 6d); occasionally, the granules, if adjacent, succeeded in giving rise to an anomalous acrosomal cap (Fig. 6g). This reveals the existence of a serious defect in intracellular trafficking/positioning of the cargo that has to be sorted to the acrosome. Another frequent anomaly was the finding of binucleate/polynucleate spermatids such as those shown in Fig. 6d, f, g. The wobbler Vps54 mutation might therefore affect cytokinesis that, although not accomplished by abscission in spermatogenic cells, always requires a functional endosome trafficking compartment (Morishita et al. 2007; Yu et al. 2007). Moreover, we observed a general disorganization of the microtubule cytoskeleton that may make the trafficking defects even worse. The positioning disorder together with microtubular defects jeopardize vesicular trafficking and the transport of organelles such as the Golgi cisternae, centrosome and mitochondria; all these events have a global effect on both the cell shape and architecture (Fig. 7a, c). Even when the spermatids were able to undergo nuclear elongation and/or form a caudal tail, the manchette exhibited an impressive organization (Fig. 7b), whereas the tail axoneme was assembled anomalously (Fig. 7d).

We then investigated, by immunogold electron microscopy, the UBPy/UBPy-sorted cargo during wobbler acrosome formation. Numerous UBPy-immunostained tubular-like structures,

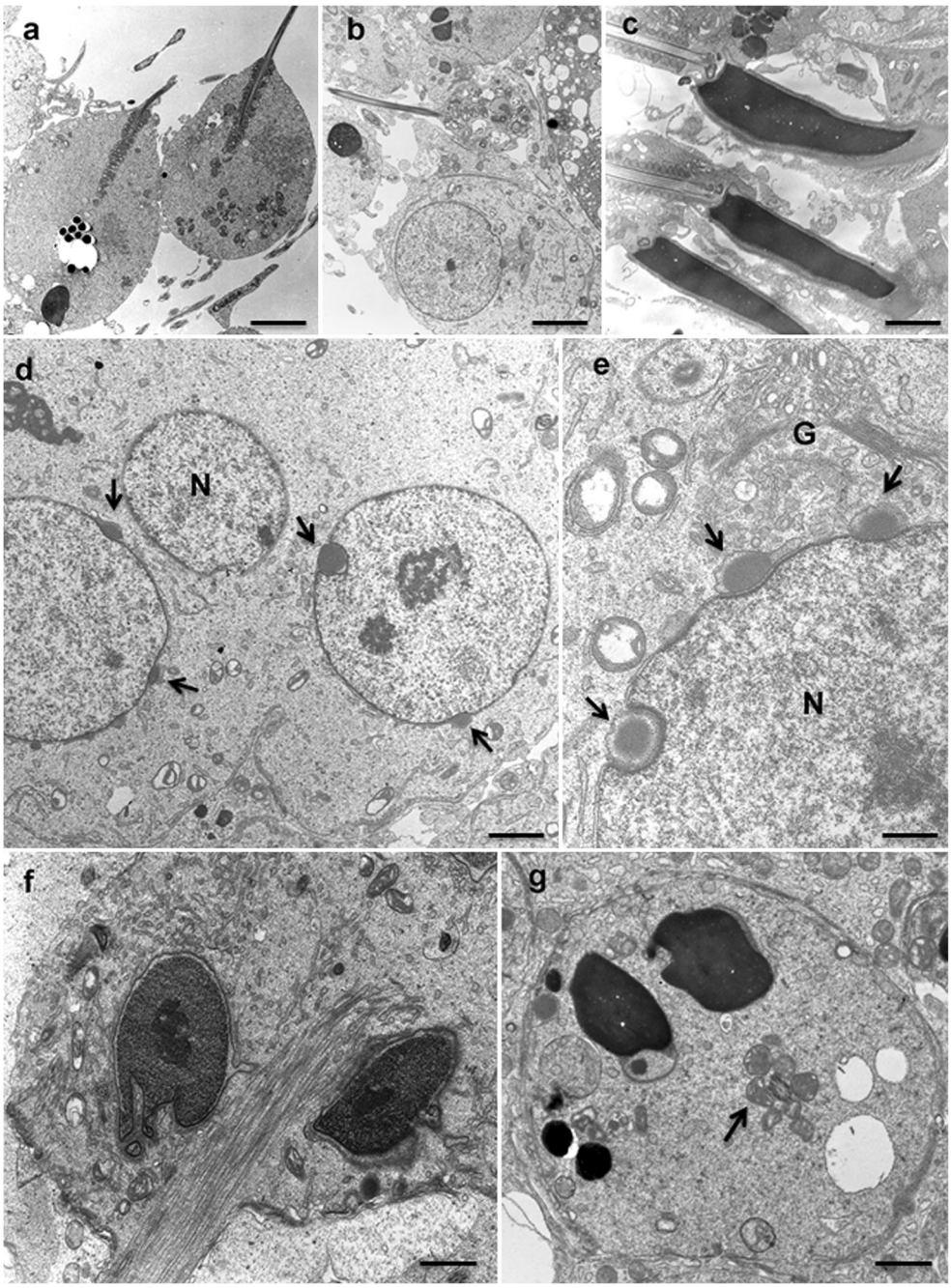

Fig. 6 Fine structure of defective spermiogenesis in the Wobbler mouse. **a**, **b** Views at low magnificataion of the luminal compartment of the seminiferous epithelium of a 34-day-old mouse. Cells proximal to the lumen and/or just released into the lumen are immature spermatids with an abnormal shape and size that have failed to elongate. The more advanced forms are characterized by a globoid head lacking an acrosome and with an anomalous nucleus and tail. *Bars* 10 μm. **c** View of the luminal compartment of a wild-type seminiferous epithelium for comparison. *Bar* 10 μm. **d** Tri-nucleate symplast of spermatids indicative of the failure of normal cytokinesis during meiotic division (*arrows* anomalous presence of multiple acrosomal granules for each spermatid). *Bar* 2 μm. **e** Higher magnification of a spermatid showing additional acrosomal granules (*arrows*) closely attached to the nucleus, an anomaly that hallmarks serious defects in trafficking/positioning. *Bar* 1 μm. **f** Bi-nucleate elongating spermatid with malformed nuclei presenting chromatin that is irregularly condensed: the dense microtubular clusters between the two nuclei represent an ectopic aberrant manchette. *Bar* 1 μm. **g** Bi-nucleate spermatid with irregular nuclei in advanced stage of chromatin condensation. Both nuclei are partially surmounted by deformed acrosomes (*arrow* transversal section of a tail middle-piece with disorganized mitochondria sheath). *Bar* 1 μm

similar to those observed in the wild-type, were recognizable inside the wobbler spermatid cytoplasm and near the nucleus (Fig. 8a). Acrosomal granules, present in more copies in the same spermatid, attached to or next to the nuclear envelope were found to be either UBPy-immunonegative (Fig. 8b) or UBPy-immunopositive (Fig. 8c). EEA1 immunogold-stained vesicles and occasional EEA1 immunogold-stained vesicular/tubular structures were detected at and near the plasma membrane and inside the spermatid cytoplasm (Fig. 8d–f); EEA1-positive acrosomal granules were rarely observed (Fig. 8e). We could not detect, by double EEA1/UBPy immunolabeling, structures that were simultaneously double-immunostained (Fig. 8g, h). As the biogenesis of the vacuole was hampered, we could not determine further significant developmental stages of the acrosome.

We have thus provided evidence that most acrosome-destined proteins cannot be sorted and/or correctly positioned in the wobbler aberrant acrosome. The RTK MET has been recently found to be UBPy-sorted to the acrosome of wild-type sperm to move subsequently to the post-acrosomal segment (PAS) in sperm that are acrosome-reacting (Berruti and Paiardi 2015).

Here, we searched for both MET and UBPy in epididymal wobbler spermatozoa by evaluating the presence of the relevant proteins by immunofluorescence analysis. As we expected, both MET and UBPy differed remarkably in their protein

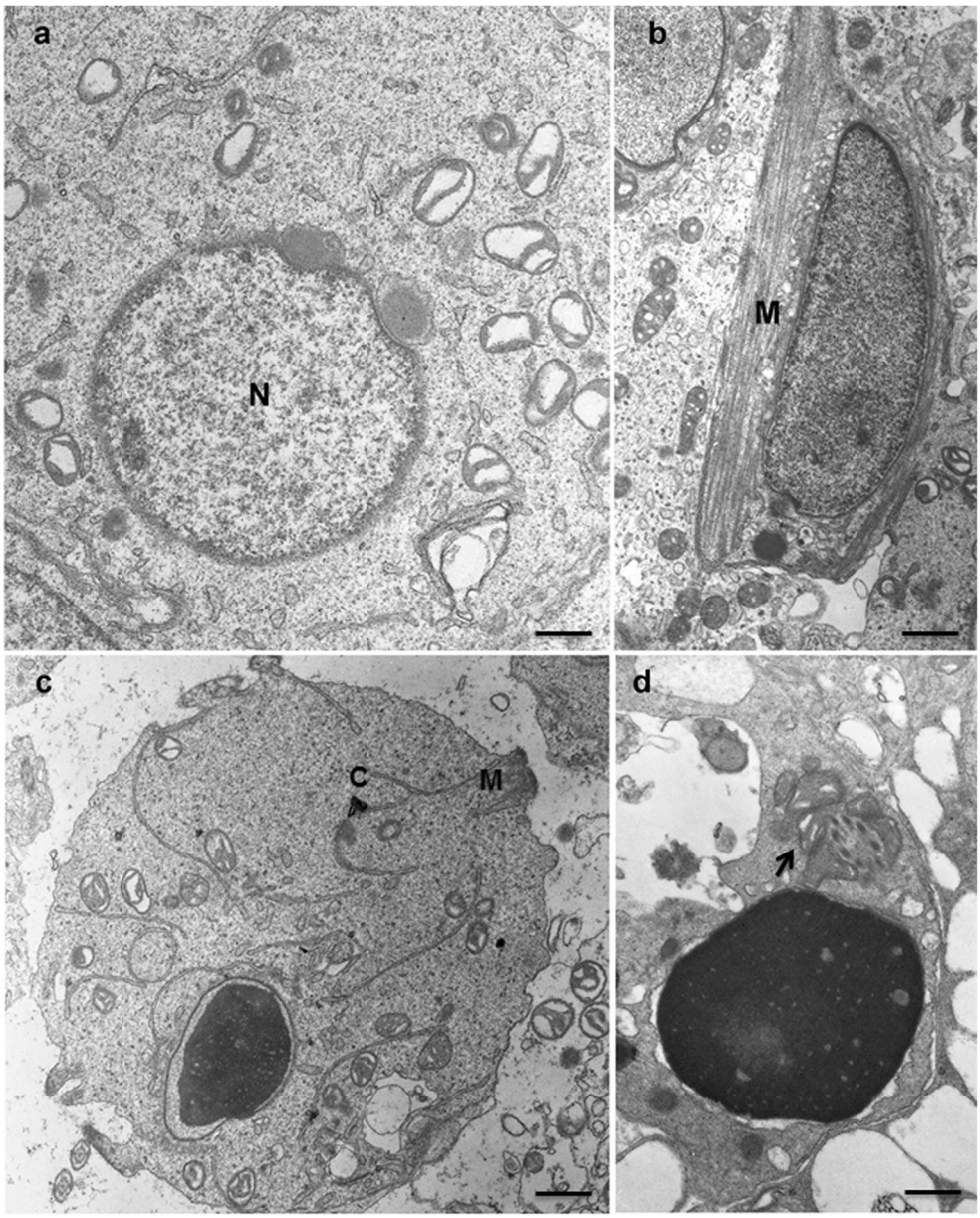

Fig. 7 General misplacement and/or disorganization of cellular organelles in wobbler spermatids. **a** Round spermatid that, in contrast to its maturation step, displays randomly dispersed Golgi cisternae and mitochondria, in addition to the abnormal presence of additional acrosomal granules. *Bar* 1.5 μm. **b** Longitudinal section of a spermatid that, nothwithstanding the elongating nucleus, is devoid of an acrosome, exhibits an ectopic and asymmetric localization of the manchette (*M*) and fails to organize a tail. *Bar* 1.5 μm. **c** Mono-nucleate spermatid with anomalously condensed chromatin, separated from the nuclear envelope engulfed in abundant cytoplasm in which recognizable long membranous profiles and a couple of centrioles (*C*) lie in abnormal positions. No signs of an acrosome or axoneme are visible. *Bar* 1.5 μm. **d** Spermatid at ripe stage of maturation. The round acrosomeless head is associated with a tail middle-piece enveloped by a dense mass of cytoplasm (*arrow* cross-section of the flagellum at its mid-piece, with disorganized mitochondria and defective axoneme). *Bar* 1.5 μm

distribution in comparison with wild-type spermatozoa. As shown in Fig. 9a, b, respectively, acrosome-less spermatozoa exhibited both proteins with a diffuse, sometimes spotted, cytoplasmic distribution; on the contrary, the double-MET/UBPy immunolabeling of wild-type spermatozoa resulted in the strict co-localization of the two proteins at the acrosome level (Fig. 9c). Consequently, MET relocation at the PAS is prevented in wobbler "fertilizing" sperm.

Discussion

Cell types equipped with unique LROs populate nascent LROs with cargoes that are diverted from endosomes. The LRO-like sperm acrosome plays essential roles in fertilization; indeed, its malformation results in substantial infertility. An improved understanding of the way that the biogenesis of the acrosome occurs might permit pathologies such as globozoospermia, for which a genetic component is involved, to be genotyped (Dam et al. 2007; Coutton et al. 2015), although the panel of genetic loci associated with the syndrome is still largely unknown. Here, we exploited, for the first time at the ultrastructural level, the contribution of the endosome compartment to the biogenesis of the acrosome.

In analogy with LROs (Raposo and Marks 2007; Lee et al. 2012; Marks et al. 2013), the biogenesis of the acrosome occurs through four distinct morphological phases. By studying trafficking phase-by-phase from EEA1-positive early endosomes and their UBPy-positive transport derivatives to the developing acrosome, we uncovered the contribution

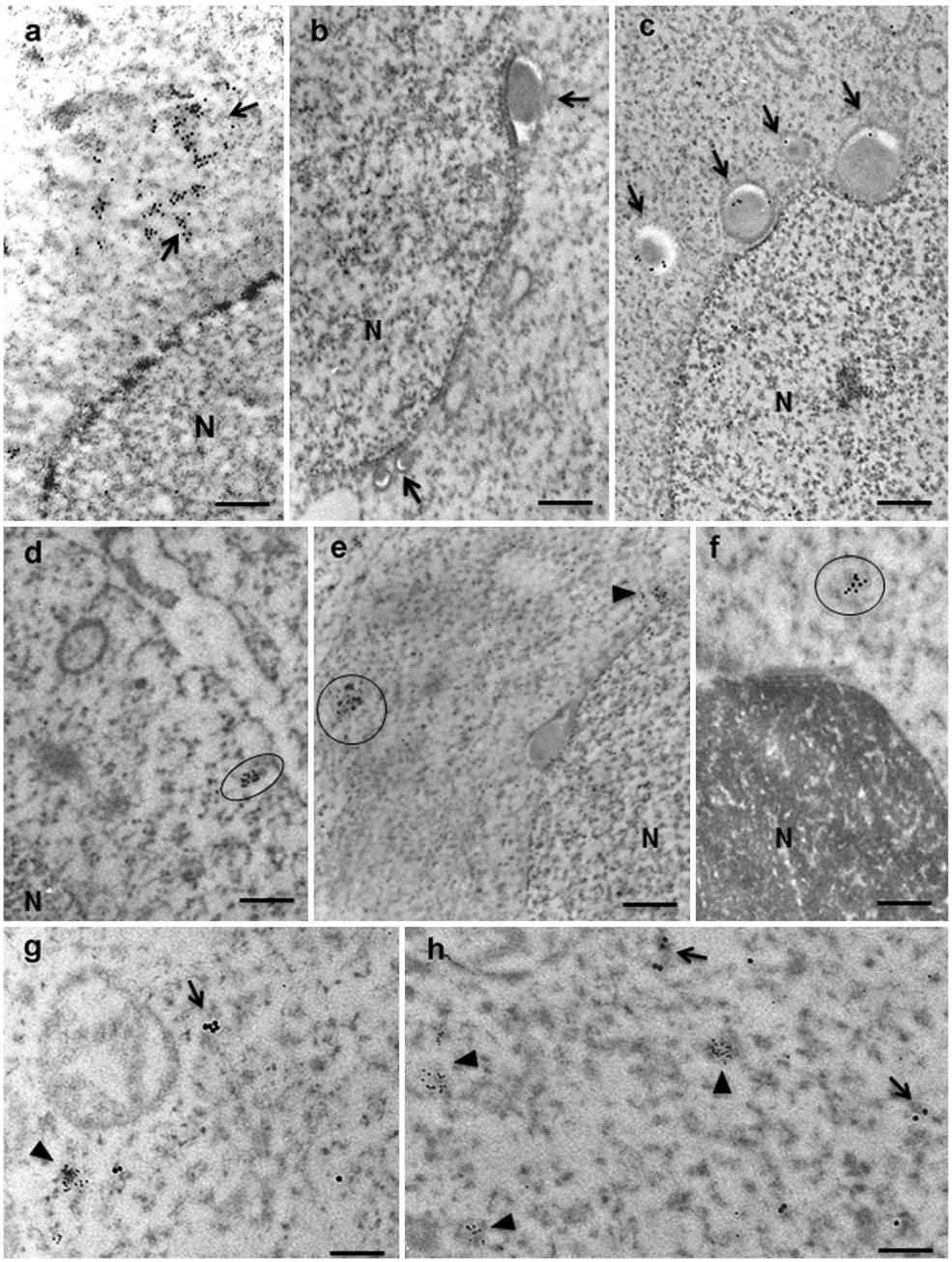

Fig. 8 Ultrastructural immunogold localization of UBPy, EEA1 and UBPy/EEA1 in wobbler spermatids. **a–c** UBPy-immunolabeling marks cytoplasmic tubular-like structures (*arrows* in **a**), whereas acrosomal granules attached or next to the nuclear envelope are immunonegative (*arrows* in **b**) or immunopositive (*arrows* in **c**) for UBPy. *Bars* 0.5 μm **d–f** EEA1-immunopositive structures are evident in the sub-plasmalemmal region (*circle* in **d**) and as tubular-like profiles inside the cytoplasm of spermatids with non-condensed and condensed chromatin (*circles* in **e**, **f**, respectively). Occasionally, EEA1-immunopositive structures are in contact with the nuclear envelope (*arrowhead* in **e**). *Bars* 0.5 μm **g**, **h** Double-immunogold localization for UBPy (15-nm gold) and EEA1 (5-nm gold). *Arrows* and *arrowheads* indicate structures immunopositive for UPBy and EEA1, respectively. *Bars* 0.5 μm

of EEA1/UBPy-sorted cargoes to the acrosome as soon as the acrosomal granule contacted the nuclear envelope via the acroplaxome (Kierszenbaum and Tres 2004). We now have to determine the sorting signal that directs this extra-Golgi material to the developing sperm vacuole. Based on the results shown here together with previous experimental evidence concerning ubiquitin ligases involved in acrosomogenesis (Rivkin et al. 2009; Zhao et al. 2013; Zimmerman et al. 2014) and anti-ubiquitin labeling during acrosome biogenesis (Haraguchi et al. 2003), we propose that such a sorting signal resides in the pattern of protein ubiquitination of the cargo diverted from endosomes to the acrosome.

One major regulatory mechanism within the endo-lysosomal system required for protein localization and fate is the post-translational protein modification by ubiquitination (Giordano et al. 2011). This modification specifies the engagement of the ubiquitinated cargo with the ESCRT transport machinery for sorting at EEA1-positive early endosomes (Mizuno et al. 2006; Berruti et al. 2010; Giordano et al. 2011). Here, UBPy, also known as the ESCRT-DUB (Wright et al. 2011), directly associates with ESCRT components, thus dictating, by modeling the ubiquitination signature of the protein cargo, the fate of the cargo that has to be sorted (Berruti 2016). We speculate that, during spermiogenesis, UBPy, which interacts with the spermatid

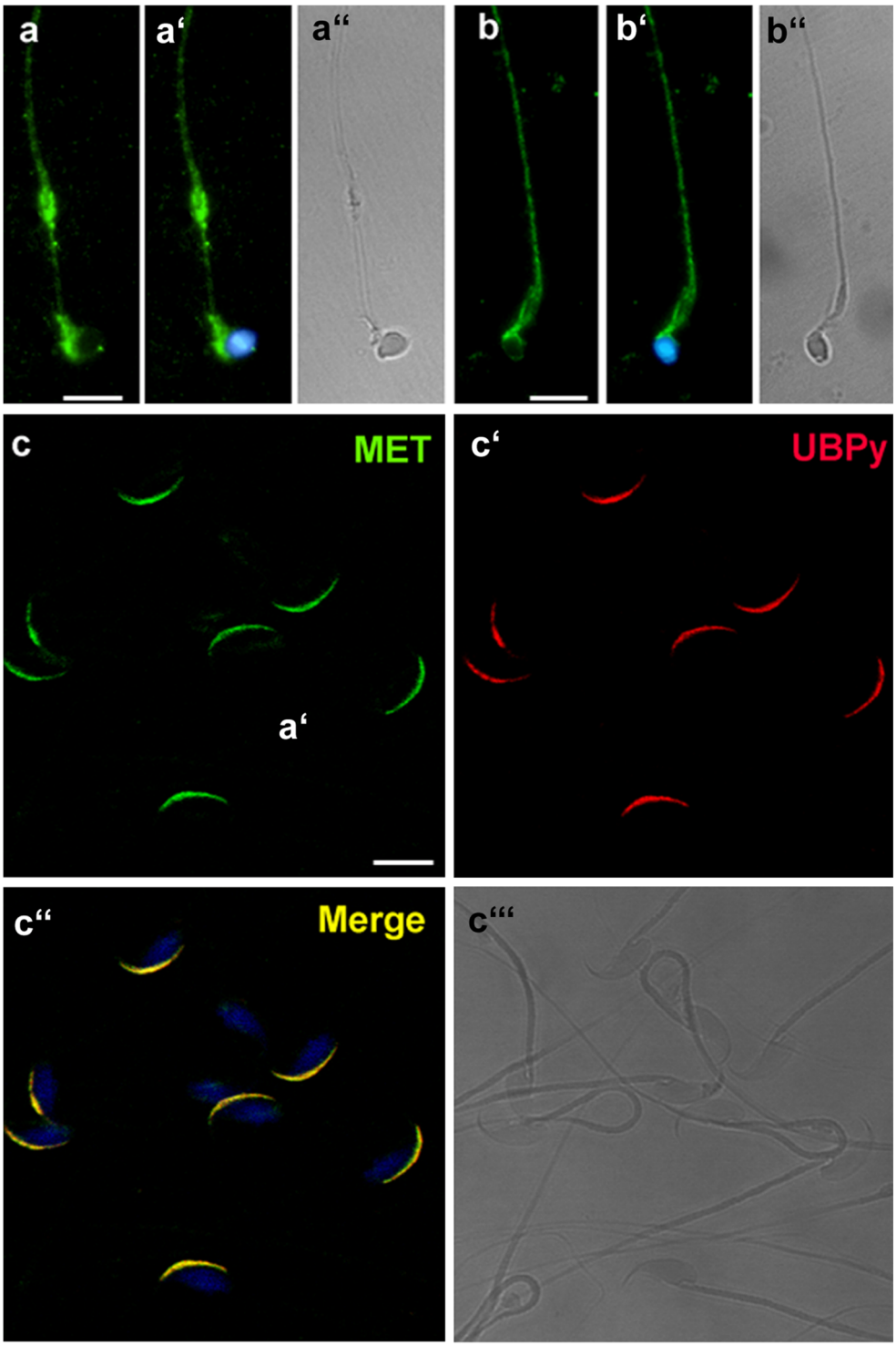

Fig. 9 Immunofluorescence of MET and UBPy in wobbler versus wild-type spermatozoa. **a**, **a'**, **b**, **b'** Wobbler epididymal spermatozoa were single-immunolabeled for MET (**a**) or UBPy (**b**) and their nuclei were counterstained with DAPI (**a'**, **b'**). **a"**, **b"** Bright field image. *Bars* 1.5 μm. **c**, **c'** Wild-type spermatozoa were simultaneously double-immunolabeled for MET (*green*) and UBPy (*red*). **c"** Triple-stained merged image (MET/UBPy/DAPI; *Merge*). **c"'** Bright field iamge. *Bar* 2 μm

ESCRT complex (Berruti et al. 2010), specifies the cargo that has to be transported from the endosomal compartment to the forming acrosome. The early endosome compartment, in particular, contains additional transport intermediates that include tubular endosomes. These last, in LRO-containing cells, are hallmarked by the BLOC-1 complex (Dell'Angelica 2004). Consistent with the interpretation of the acrosome as a LRO, we checked for the presence of pallidin, which is the BLOC-1 component that interacts with the early endosome t-SNARE syntaxin-13 (Cullinane et al. 2011). Although never described in male germ cells, we first assayed pallidin by basic analyses such as Western immunoblot and immunofluorescence. Spermatids expressed pallidin, which exhibited the expected molecular size and a spotted intracellular localization in agreement with the BLOC-1/pallidin localization

described in melanocytes (Setty et al. 2007; Raposo and Marks 2007). Immunoelectron microscopy revealed that the pallidin signature was consistent with that of UBPy during acrosomogenesis. Hence, in spermatids, pallidin might be involved in diverting selective cargoes from early endosomes to the acrosome.

Like the melanosome matrix (Sitaram and Marks 2012), the acrosomal matrix exhibits self-aggregation properties that lead, at the late acrosomogenic phases, to acrosome compaction with a dense-core scaffold; the last-mentioned represents a stable platform for the sequential release of matrix-associated proteins during the acrosome reaction. We found that the scaffold is devoid of UBPy immunogold particles, whereas these always delineated the profiles of the inner and outer acrosomal membrane, particularly at the equatorial segment. This finding suggests that UBPy-sorted cargoes are recruited at the acrosome for the assemblage of selected membrane microdomains. Accumulating evidence indicates that the acrosome is not only a "bag of enzymes" used to penetrate the oocyte's investments but also might perform other roles. As is known, the mechanisms of membrane protein relocation, possibly guided by scaffold-associated proteins, promote the clustering of constituents of a signaling pathway in liquid-ordered membrane microdomains (Tsui-Pierchala et al. 2002). Similar mechanisms might also operate at the acrosome level; hence, even when it is reacting/has reacted at fertilization, the acrosome might still provide molecules involved in sperm-oocyte fusion and/or oocyte activation. Izumo, the acrosomal protein responsible for sperm-egg fusion, redistributes to the surface of the equatorial segment in fertilizing sperm (Satouh et al. 2012), whereas phospholipase C zeta (PLCζ), the most quoted as the sperm factor that triggers oocyte activation (Saunders et al. 2002), relocates at the PAS. PLCζ has, however, to be activated through tyrosine phosphorylation to generate the movement of Ca^{2+} transients into the ooplasm, being in an inactive state at the acrosome of ejaculated sperm (Amdani et al. 2013).

Globozoospermia in humans is a rare and severe teratozoospermia consisting primarily of spermatozoa lacking an acrosome. Familial cases of globozoospermia have suggested a genetic basis; in spite of the complexity and multitude of proteins involved in acrosome biogenesis, however, only a few spontaneous mutations have been so far identified as responsible for globozoospermia in humans (Dam et al. 2007; Koscinski et al. 2011; Coutton et al. 2015). Conversely, as reviewed by Coutton et al. (2015), more than 50 genetically lab-modified mice reported in the Mouse Genome Informatics database (http://www.informatics.jax.org) exhibit a globozoospermia-like phenotype. Within this wide spectrum, the wobbler mouse is a good experimental model for several features, including its globozoospermia attributable to a spontaneous recessive mutation that changes a highly conserved leucine into a glutamine (Schmitt-John et al. 2005) in the protein region crucial for mediating the Vps54 localization to early endosomes (Quenneville et al. 2006). Moreover, wobbler spermatozoa even fail to fertilize oocytes after ICSI, unlike other mouse KO-mutants with a globozoospermia-like phenotype. Such unsuccessful oocyte-activation capacity has been ascribed to the abnormal localization of PLCζ (Heytens et al. 2010), just as has been shown to occur for ICSI-infertile globozoospermic men with mislocalized PLCζ (Escoffier et al. 2015). Here, we provide detailed documentation for the derailment of acrosome biogenesis in the Vps54 mouse mutant. The results from our electron microscopy study are supported by our immunogold electron microscopy analysis. Taken together, our findings revealed that the acrosome does not develop because of the malfunctioning of the retrograde vesicular traffic that, in turn, hampers the correct contribution of protein cargoes, in particular from the endosomal compartment. In the wobbler mouse, acrosome biogenesis apparently stops at a phase approximately evaluated as an early cap phase; the lack of a real acrosome is, consequently, attributable neither to acrosome fragmentation as for the GOPC-KO mouse (Yao et al. 2002), nor to acrosome detachment/lack of attachment from/to the nuclear envelope, as for Csk2a2-KO and Dpy19l2-KO/SPACA1-KO mice, respectively, (Xu et al. 1999; Pierre et al. 2012; Fujihara et al. 2012). Furthermore, wobbler trafficking defects do not hit acrosome biogenesis only; other critical events, dependent on microtubule-mediated trafficking, such as cytokinesis, intramanchette and intraflagellar transport and spermatid shaping, are affected. As a last consideration, we suggest that the lack of the correct contribution from the endosome compartment results in the non-delivery of the UBPy-sorted cargo to the acrosome. Our immunofluorescence findings provide evidence that, in wobbler epididymal spermatozoa, both the RTK MET and UBPy are mislocalized, and that, consequently, the receptor cannot relocate at the PAS at fertilization as it does in wild-type spermatozoa (Berruti 2016). Possibly, wobbler (Heytens et al. 2010) and human wobbler-like (Escoffier et al. 2015) globozoospermic phenotypes are infertile, even after ICSI, because their sperm PLCζ is not only mislocalized but also cannot be appropriately activated by a potential PLCζ activator as is MET.

Given the exclusive nature of the mammalian sperm acrosome, further analysis of ubiquitin-dependent cargo-sorting during acrosome biogenesis will offer a unique opportunity to dissect, from a general point of view, the functional meaning of a specific type of protein ubiquitination within the endocytic system of a mammalian cell.

Acknowledgments This work was financially supported by Transition Grant 2012, University of Milan, to Giovanna Berruti.

Compliance with ethical standards

Conflict of interest The authors declare that they have no conflict of interest.

References

Amdani SN, Jones C, Coward K (2013) Phospholipase C zeta (PLCζ): oocyte activation and clinical links to male factor infertility. Adv Biol Regul 53:292–308

Berruti G (2016) Towards defining an "origin"—the case for the mammalian acrosome. Semin Cell Dev Biol 59:46–53. doi:10.1016/j.semcdb.2016.01.013

Berruti G, Martegani E (2005) The deubiquitinating enzyme mUBPy interacts with the sperm-specific molecular chaperone MSJ-1: the relation with the proteasome, acrosome, and centrosome in mouse male germ cells. Biol Reprod 72:14–21

Berruti G, Paiardi C (2011) Acrosome biogenesis: revisiting old questions to yield new insights. Spermatogenesis 1:95–98

Berruti G, Paiardi C (2015) USP8/UBPy-regulated sorting and the development of sperm acrosome: the recruitment of MET. Reproduction 149:633–644

Berruti G, Ripolone M, Ceriani M (2010) USP8, a regulator of endosomal sorting, is involved in mouse acrosome biogenesis through interaction with the spermatid ESCRT-0 complex and microtubules. Biol Reprod 82:930–939

Boillée S, Berruti G, Meccariello R, Grannec G, Razan F, Pierantoni R, Fasano S, Junier MP (2002) Early defect in the expression of mouse sperm DNAJ 1, a member of the DNAJ/heat shock protein 40 chaperone protein family, in the spinal cord of the wobbler mouse, a murine model of motoneuronal degeneration. Neuroscience 113: 825–835

Buffone MG, Foster JA, Gerton GL (2008) The role of the acrosomal matrix in fertilization. Int J Dev Biol 52:511–522

Ceriani M, Amigoni L, D'Aloia A, Berruti G, Martegani E (2015) The deubiquitinating enzyme UBPy/USP8 interacts with TrkA and inhibits neuronal differentiation in PC12 cells. Exp Cell Res 333:49–59

Coutton C, Escoffier J, Martinez G, Arnoult C, Ray PF (2015) Teratozoospermia: spotlight on the main genetic actors in the human. Hum Reprod Update 21:455–85

Cullinane AR, Curry JA, Carmona-Rivera C, Summers CG, Ciccone C, Cardillo ND, Dorward H, Hess RA, White JG, Adams D, Huizing M, Gahl WA (2011) A BLOC-1 mutation screen reveals that PLDN is mutated in Hermansky-Pudlak syndrome type 9. Am J Hum Genet 88:778–787

Dam AH, Koscinski I, Kremer JA, Moutou C, Jaeger AS, Oudakker AR, Tournaye H, Charlet N, Lagier-Tourenne C, Bokhoven H van, Viville S (2007) Homozygous mutation in *SPATA16* is associated with male infertility in human globozoospermia. Am J Hum Genet 81:813–820

Dell'Angelica EC (2004) The building BLOC(k)s of lysosomes and related organelles. Curr Opin Cell Biol 16:458–464

Escoffier J, Yassine S, Lee HC, Martinez G, Delaroche J, Coutton C, Karaouze'ne T, Zouari R, Metzler-Guillemain C, Pernet-Gallay K, Hennebicq S, Pierre F, Ray PF, Fissore R, Arnoult C (2015) Subcellular localization of phospholipase Cz in human sperm and its absence in DPY19L2-deficient sperm are consistent with its role in oocyte activation. Mol Hum Reprod 21:157–168

Falcón-Pérez JM, Starcevic M, Gautam R, Dell'Angelica EC (2002) BLOC-1, a novel complex containing the pallidin and muted proteins involved in the biogenesis of melanosomes and platelet-dense granules. J Biol Chem 277:28191–28199

Fujihara Y, Satouh Y, Inoue N, Isotani A, Ikawa M, Okabe M (2012) SPACA1-deficient male mice are infertile with abnormally shaped sperm heads reminiscent of globozoospermia. Development 139: 3583–3589

Giordano F, Simoes S, Raposo G (2011) The ocular albinism type 1 (OA1) GPCR is ubiquitinated and its traffic requires endosomal sorting complex responsible for transport (ESCRT) function. Proc Natl Acad Sci 108:11906–11911

Gnesutta N, Ceriani M, Innocenti M, Mauri I, Zippel R, Sturani E, Borgonovo B, Berruti G, Martegani E (2001) Cloning and characterization of mouse UBPY, a deubiquitinating enzyme that interacts with the ras guanine nucleotide exchange factor CDC25(Mm)/Ras-GRF1. J Biol Chem 276:39448–39454

Guyonnet B, Zabet-Moghaddam M, SanFrancisco S, Cornwall GA (2012) Isolation and proteomic characterization of the mouse sperm acrosomal matrix. Mol Cell Proteomics 11:758–774

Haraguchi CM, Mabuchi T, Hirata S, Shoda T, Hoshi K, Yokota S (2003) Ubiquitin signals in the developing acrosome during spermatogenesis of rat testis: an immunoelectron microscopic study. Histochem Cell Biol 120:63–71

Hardy DM, Oda MN, Friend DS, Huang TT Jr (1991) A mechanism for differential release of acrosomal enzymes during the acrosome reaction. Biochem J 275:759–766

Heimann P, Laage S, Jockusch H (1991) Defect of sperm assembly in a neurological mutant of the mouse, wobbler (WR). Differentiation 47:77–83

Heytens E, Schmitt-John T, Moser JM, Jensen NM, Soleimani R, Young C, Coward K, Parrington J, De Sutter P (2010) Reduced fertilization after ICSI and abnormal phospholipase C zeta presence in spermatozoa from the wobbler mouse. Reprod Biomed Online 21:742–749

Ito C, Yamatoya K, Yoshida K, Kyono K, Yao R, Noda T, Toshimori K (2010) Appearance of an oocyte activation-related substance during spermatogenesis in mice and humans. Hum Reprod 25:2734–2744

Jockusch H, Holland A, Staunton L, Schmidt-John T, Heimann P, Dowling P, Ohlendiek K (2014) Pathoproteomics of testicular tissue deficient in the GARP component VPS54: the wobbler mouse model of globozoospermia. Proteomics 14:839–852

Kierszenbaum AL, Tres LL (2004) The acrosome-acroplaxome-manchette complex and the shaping of the spermatid head. Arch Histol Cytol 67:271–284

Koscinski I, Elinati E, Fossard C, Redin C, Muller J, Velez de la Calle J, Schmitt F, Ben Khelifa M, Ray PF, Kilani Z, Barratt CL, Viville S (2011) DPY19L2 deletion as a major cause of globozoospermia. Am J Hum Genet 88:344–350

Kosova G, Scott NM, Niederberger C, Prins GS, Ober C (2012) Genome-wide association study identifies candidate genes for male fertility traits in humans. Am J Hum Genet 90:950–961

Lee HH, Nemecek D, Schindler C, Smith WS, Ghirlando R, Steven AC, Bonifacino JS, Hurley JH (2012) Assembly and architecture of biogenesis of lysosome-related organelles complex-1 (BLOC-1). J Biol Chem 287:5882–5890

Li W, Rusiniak ME, Chintala S, Gautam R, Novak EK, Swank RT (2004) Murine Hermansky-Pudlak syndrome genes: regulators of lysosome-related organelles. Bioessays 26:616–628

Marks MS, Heijnen HF, Raposo G (2013) Lysosome-related organelles: unusual compartments become mainstream. Curr Opin Cell Biol 25: 495–505

Meng R, Wang Y, Yao Y, Zhang Z, Harper DC, Heijnen HF, Sitaram A, Li W, Raposo G, Weiss MJ, Poncz M, Marks MS (2012) SLC35D3 delivery from megakaryocyte early endosomes is required for platelet dense granule biogenesis and is differentially defective in Hermansky-Pudlak syndrome models. Blood 120:404–414

Mizuno E, Kobayashi K, Yamamoto A, Kitamura N, Komada M (2006) A deubiquitinating enzyme UBPY regulates the level of protein ubiquitination on endosomes. Traffic 7:1017–1031

Moreno RD, Ramalho-Santos J, Sutovsky P, Chan EK, Schatten G (2000) Vesicular traffic and Golgi apparatus dynamics during mammalian spermatogenesis: implications for acrosome architecture. Biol Reprod 63:89–98

Morishita M, Mendonsa R, Wright J, Engebrecht J (2007) Snc1p v-SNARE transport to the prospore membrane during yeast

sporulation is dependent on endosomal retrieval pathways. Traffic 8: 1231–1245

Paiardi C, Pasini ME, Gioria M, Berruti G (2011) Failure of acrosome formation and globozoospermia in the wobbler mouse, a Vps54 spontaneous recessive mutant. Spermatogenesis 1:52–62

Paiardi C, Pasini ME, Amadeo A, Gioria M, Berruti G (2014) The ESCRT-deubiquitinating enzyme USP8 in the cervical spinal cord of wild-type and Vps54 recessive (wobbler) mutant mice. Histochem Cell Biol 141:57–73

Pierre V, Martinez G, Coutton C, Delaroche J, Yassine S, Novella C, Pernet-Gallay K, Hennebicq S, Ray PF, Arnoult C (2012) Absence of Dpy19l2, a new inner nuclear membrane protein, causes globozoospermia in mice by preventing the anchoring of the acrosome to the nucleus. Development 139:2955–2965

Quenneville NR, Chao TY, McCaffery JM, Conibear E (2006) Domains within the GARP subunit Vps54 confer separate functions in complex assembly and early endosome recognition. Mol Biol Cell 17: 1859–1870

Raposo G, Marks MS (2007) Melanosomes—dark organelles enlighten endosomal membrane transport. Nat Rev Mol Cell Biol 8:786–797

Rivkin E, Kierszenbaum AL, Gil M, Tres LL (2009) Rnf19a, a ubiquitin protein ligase, and Psmc3, a component of the 26S proteasome, tether to the acrosome membranes and the head-tail coupling apparatus during rat spermatid development. Dev Dyn 238:1851–1861

Satouh Y, Inoue N, Ikawa M, Okabe M (2012) Visualization of the moment of mouse sperm-egg fusion and dynamic localization of IZUMO1. J Cell Sci 125:4985–4990

Saunders CM, Larman MG, Parrington J, Cox LJ, Royse J, Blayney LM, Swann K, Lai FA (2002) PLCζ: a sperm-specific trigger of Ca^{2+} oscillations in eggs and embryo development. Development 129: 3533–3544

Schmitt-John T, Drepper C, Mussmann A, Hahn P, Kuhlmann M, Thiel C, Hafner M, Lengeling A, Heimann P, Jones JM, Meisler MH, Jockusch H (2005) Mutation of Vps54 causes motor neuron disease and defective spermiogenesis in the wobbler mouse. Nat Genet 37: 1213–1215

Setty SR, Tenza D, Truschel ST, Chou E, Sviderskaya EV, Theos AC, Lamoreux ML, Di Pietro SM, Starcevic M, Bennett DC, Dell'Angelica EC, Raposo G, Marks MS (2007) BLOC-1 is required for cargo-specific sorting from vacuolar early endosomes toward lysosome-related organelles. Mol Biol Cell 18:768–780

Sitaram A, Marks MS (2012) Mechanisms of protein delivery to melanosomes in pigment cells. Physiology (Bethesda) 27:85–99

Spiegel S, Chiu A, James AS, Jentsch JD, Karlsgodt KH (2015) Recognition deficits in mice carrying mutations of genes encoding BLOC-1 subunits pallidin or dysbindin. Genes Brain Behav 14: 618–624

Tsui-Pierchala BA, Encinas M, Milbrandt J, Johnson EM Jr (2002) Lipid rafts in neuronal signaling and function. Trends Neurosci 25:412–417

Vanden Meerschaut F, Nikiforaki D, De Roo C, Lierman S, Qian C, Schmitt-John T, De Sutter P, Heindryckx B (2013) Comparison of pre- and post-implantation development following the application of three artificial activating stimuli in a mouse model with round-headed sperm cells deficient for oocyte activation. Hum Reprod 28:1190–1198

Wang H, Wan H, Li X, Liu W, Chen Q, Wang Y, Yang L, Tang H, Zhang X, Duan E, Zhao X, Gao F, Li W (2014) Atg7 is required for acrosome biogenesis during spermatogenesis in mice. Cell Res 24:852–869

Wright MH, Berlin I, Nash PD (2011) Regulation of endocytic sorting by ESCRT-DUB-mediated deubiquitination. Cell Biochem Biophys 60:39–46

Xu X, Toselli PA, Russell LD, Seldin DC (1999) Globozoospermia in mice lacking the casein kinase II alpha' catalytic subunit. Nat Genet 23:118–121

Yanagimachi R (2011) Mammalian sperm acrosome reaction: where does it begin before fertilization. Biol Reprod 85:4–5

Yao R, Ito C, Natsume Y, Sugitani Y, Yamanaka H, Kuretake S, Yanagida K, Sato A, Toshimori K, Noda T (2002) Lack of acrosome formation in mice lacking a Golgi protein, GOPC. Proc Natl Acad Sci U S A 99:11211–11216

Yu X, Prekeris R, Gould GW (2007) Role of endosomal Rab GTPases in cytokinesis. Eur J Cell Biol 86:25–35

Zhao B, Ito K, Iyengar PV, Hirose S, Nakamura N (2013) MARCH7 E3 ubiquitin ligase is highly expressed in developing spermatids of rats and its possible involvement in head and tail formation. Histochem Cell Biol 139:447–460

Zimmerman SW, Yi YJ, Sutovsky M, Leeuwen FW van, Conant G, Sutovsky P (2014) Identification and characterization of RING-finger ubiquitin ligase UBR7 in mammalian spermatozoa. Cell Tissue Res 356:261–278